

# JOURNAL OF ADVANCED APPLIED SCIENCES

IENCES PRENSIP

https://prensip.gen.tr

e-ISSN: 2979-9759

## RESEARCH ARTICLE

# The Mechanical Modelling of CoFe<sub>2</sub>O<sub>4</sub> doped Y123 Superconductor

Elif Asikuzun Tokeser<sup>1™</sup> • Fatih Bulut<sup>2</sup> • Abdulrahman Nefrow<sup>3</sup>

• Turgay Seydioglu<sup>4</sup> • Sedat Kurnaz<sup>5</sup> •

<sup>1</sup>Kastamonu University, Faculty of Engineering and Architecture, Department of Metallurgical and Materials Engineering, Kastamonu/Türkiye

<sup>2</sup>Sinop University, Scientific and Technological Research Applications and Research Center, Sinop/Türkiye

<sup>3</sup>Kastamonu University, Institute of Science, Department of Electrical and Electronics Engineering, Kastamonu/Türkiye

#### ARTICLE INFO

#### **Article History**

Received: 09.05.2023 Accepted: 15.06.2023 First Published: 30.06.2023

#### **Keywords**

Sol-gel Solid state Vickers Y123



#### **ABSTRACT**

In the current work, the load-independent Vickers hardness values of  $CoFe_2O_4$  doped Y123 compounds were investigated by using six mechanical modeling approaches namely law of Meyer Law, proportional sample resistance (PSR), elastic/plastic deformation (EPD), proportional sample resistance (PSR), Hays-Kendall (HK) and indentation induced cracking (IIC). Solid state reaction and the sol gel methods were preferred to produce samples undoped and  $CoFe_2O_4$  doped. Vickers microhardness tests were conducted on samples with loads of F=0.249, 0.450, 0.980, 1.990, and 2.940 N in order to ascertain the influence of  $CoFe_2O_4$  particles on the general mechanical properties of the Y123 matrix. While the HK approach was the most suitable model for samples exhibiting ISE behavior, the IIC model was determined as the most successful model for samples exhibiting RISE behavior.

# Please cite this paper as follows:

Asikuzun Tokeser, E., Bulut, F., Nefrow, A., Seydioglu, T., & Kurnaz, S. (2023). The mechanical modelling of CoFe<sub>2</sub>O<sub>4</sub> doped Y123 superconductor. *Journal of Advanced Applied Sciences*, 2(1), 1-14. https://doi.org/10.29329/jaasci.2023.562.01

## 1. Introduction

A well-known ceramic superconductor called  $YBa_2Cu_3O_{7-\delta}$  (also known as YBCO-123 or Y-123) passes through the superconducting transition at 92 K. While YBCO and other high-temperature superconductors show great promise for a variety of real-world applications, they are constrained by their brittle mechanical characteristics, which are caused by the inherent layered structure of ceramics and the inevitable presence of porosity in sintered samples. Numerous studies

have investigated the use of different additives to improve the structural, electrical, magnetic, and mechanical properties of YBCO ceramic superconductors in an effort to address this problem (Feng et al., 1994; Leblond-Harnois et al., 2000).

Due to their remarkable superconducting properties, which make them viable candidates for a variety of practical applications, superconducting materials, such as YBaCuO ceramics, have been studied in great detail. Their mechanical characteristics, especially at cryogenic temperatures,

E-mail address: easikuzun@kastamonu.edu.tr

<sup>&</sup>lt;sup>4</sup>Kastamonu University, Kastamonu Vocational School, Department of Electronics and Automation, Kastamonu/Türkiye

<sup>&</sup>lt;sup>5</sup>Kastamonu University, Central Research Laboratory, Kastamonu/Türkiye

<sup>&</sup>lt;sup>™</sup> Corresponding author

frequently, though, limit their possible use by increasing sample size, melt-textured materials, for instance, can show improved field-trapping properties; however, the resulting strong magnetic forces and flux density gradients can produce complex stress fields that could lead to the material breaking (Leblond-Harnois et al., 2000). Furthermore, YBaCuO materials are brittle ceramics with weak microstructure regions that can lead to localized stress concentrations and ultimate sample cracking. Due to tension brought on during the cooling process from the processing temperature and during oxygenation, microcracks are also frequently present. Therefore, the poor mechanical performance of these materials frequently restricts their practical uses (Turkoz et al., 2013).

When a force is applied, a material's capacity to deform or oppose deformation determines how it will behave mechanically (Khalil, 2001; Koralay et al., 2014). Elastic and plastic deformation are the two different kinds. While plastic deformation is permanent and happens when the force applied surpasses the material's elasticity limit, elastic deformation is transient and does not cause atom separation. The ability of a material to withstand friction, scratching, cutting, and plastic deformation is known as hardness. Because it is straightforward and causes little harm to the sample, hardness measurement is a popular and efficient method for determining the mechanical characteristics of materials. Furthermore, because hardness is closely correlated with other mechanical characteristics like tensile strength, measuring hardness can provide insight into a material's strength (Aydiner et al., 2010).

Using both the solid-state reaction and the sol-gel techniques, we have created a composite superconductor in this research with the intention of examining how the doping CoFe2O4 affects the superconducting, structural and mechanical properties of YBCO. Specifically, we will discuss the observed load-independent micro-hardness behavior of the data by fitting it to different approaches from the literature before presenting the results of micro-indentation hardness measurements.

## 2. Materials and Methods

CoFe<sub>2</sub>O<sub>4</sub> doping Y123 superconducting samples were prepared in this research using two different approaches. For the samples created by the SSR technique and the SG method, CoFe<sub>2</sub>O<sub>4</sub> (30 nm nano sized powder (observed by TEM) purchased from Sigma) was used as the doping substance. Precursor powders of Y<sub>2</sub>O<sub>3</sub>, BaCO<sub>3</sub>, and CuO were preferred for the SSR technique of producing samples. In the SG technique, barium acetate powder was mixed at room temperature with 15 mL of acetic acid and methanol anhydrous. The obtained homogeneous barium mixture was then re-mixed with the yttrium acetate and copper acetate respectively and 8 mL of triethanolamine added the homogenous mixture. Triethanolamine is used to hasten copper's decomposition

process. The cup was opened, the obtained turquoise homogenous solution was stirred for 12 hours at room temperature, and then the solution was heated to 80 °C to cause it to gel. The solution was baked at 300 °C for 30 minutes to give it a gel-like consistency.

For the production of the samples in the chosen phase, starting powders were weighed in this research using 1:2:3 stoichiometric ratios. The weight-based doping ratio for the YBa<sub>2</sub>Cu<sub>3-x</sub>(CoFe<sub>2</sub>O<sub>4</sub>)<sub>x</sub>O<sub>7</sub> structure was set at 0 to 20%. The stoichiometrically weighted beginning powders were first ground for an hour in an agate mortar. Three times, the powder combination was calcined at 850 °C for one day in a cube furnace using alumina boats. CoFe<sub>2</sub>O<sub>4</sub> was incorporated into blended powders at 0%, 0.05%, 0.10%, and 0.20% weight percentages. Using a hydraulic press, the powders were compressed into discs with diameters of 10 mm in diameter and 2 mm in thickness. The examples were annealed in air for 24 hours at a temperature of 930 °C, then cooled to 500 °C and exposed to oxygen for 5 hours. Samples which obtained after calcination were named as SSR-0, SSR-5, SSR-10, SSR-20 for SSR method and SG-0, SG-5, SG-10, SG-20 for sol-gel method.

#### 3. Results and Discussion

## 3.1. Structural Analysis

Figure 1 shows the XRD patterns of the specimens prepared using the SSR and SG methods. For the sample prepared using these techniques, the peak intensities dropped and the peaks shifted to smaller angles as the doping ratio increased. This is explained by how the doping affects the crystallinity of the prepared samples. We can conclude that Co+2 ions were effectively replaced with Fe<sup>+2</sup> and Co<sup>+3</sup> ions or were included in the Y123 structure because impurity peaks relevant with Fe or Co are not observed.

The a, b and c lattice parameters were obtained for orthomorphic structure by Eq.1.

$$\frac{1}{d^2} = \frac{h^2}{a^2} + \frac{k^2}{b^2} + \frac{l^2}{c^2} \tag{1}$$

$$D = \frac{0.941 \,\lambda}{B \cos \,\theta} \tag{2}$$

$$B^2 = B_s^2 - B_m^2 (3)$$

$$\delta = 100(a-b)/(a+b) \tag{4}$$

The values for the samples' particle sizes were calculated using Eqs. 2 and 3. According to the, the calculated lattice parameters, grain sizes, orthorombicity value (determined by Eq. 4) shifting of peaks to lower angles and reduction in peak intensities are all listed in Table 1. According to the literature, the Y-123 superconducting phase's lattice parameters are a=3.82, b=3.88, and c=11.69 (Yeoh & Ahmad, 2008; Yilmaz & Dogan, 2012). The lattice parameters of the study's samples



have values that are compatible with those in the literature. Yet, doping the samples results in modifications to the lattice parameters, proving that the doping has an impact on the material's crystal structure. Particle size values for SSR samples changed due to doping, with the exception of SSR-20. Particle

size did not vary in a predictable way in samples made using the sol-gel technique. While the SG method's lowest doping induced an increase in particle size, a subsequent rise in the doping level led to a decrease in particle size.

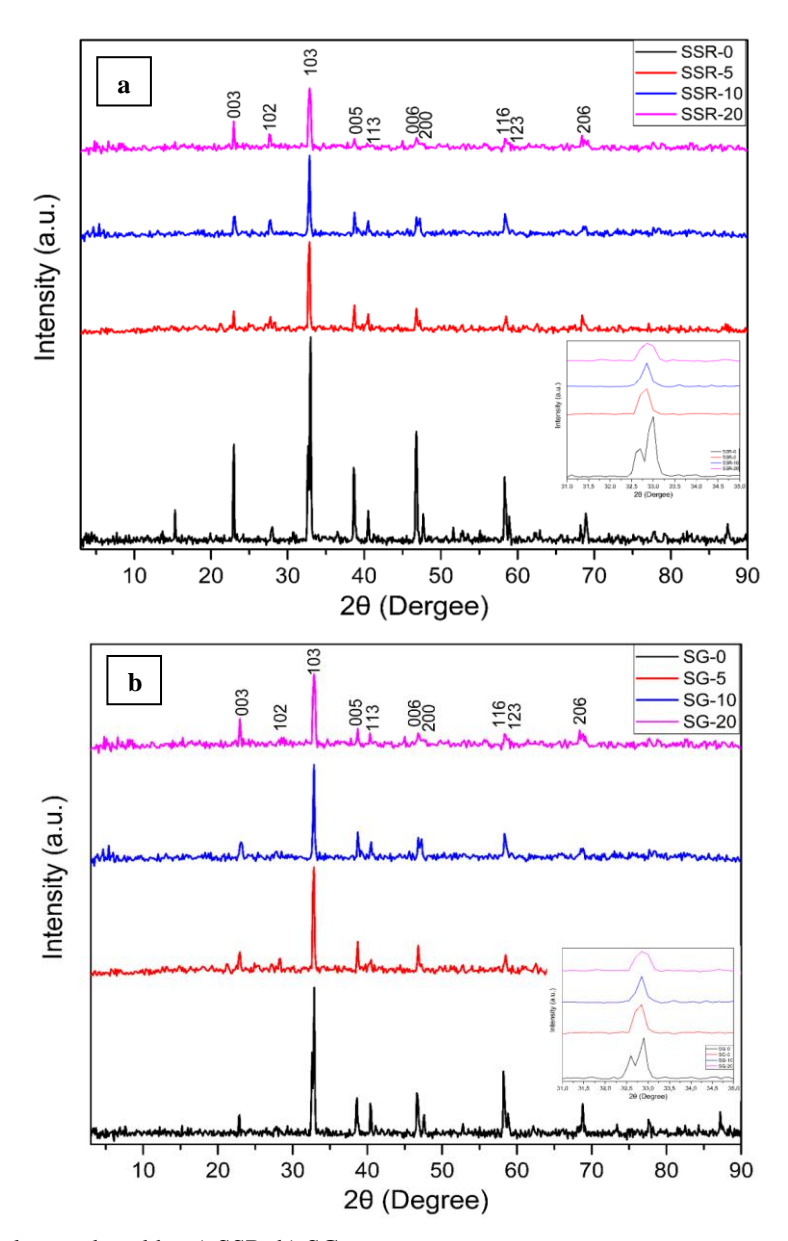


Figure 1. XRD graphs of samples produced by a) SSR, b) SG.

Table 1. Structural parameters from XRD analysis.

| Sample        | Grain Size (Å) | a (Å) | b (Å) | c (Å)  | Volume (V) | Orthorombicity $(\delta)$ |
|---------------|----------------|-------|-------|--------|------------|---------------------------|
| SSR-0         | 28.95          | 3.815 | 3.882 | 11.683 | 173.023    | 0.8705                    |
| SSR-5         | 30.16          | 3.821 | 3.872 | 11.633 | 172.109    | 0.6629                    |
| <b>SSR-10</b> | 30.78          | 3.813 | 3.874 | 11.629 | 171.778    | 0.7936                    |
| SSR-20        | 24.53          | 3.810 | 3.855 | 11.614 | 170.581    | 0.5871                    |
| SG-0          | 28.21          | 3.822 | 3.898 | 11.619 | 173.102    | 0.9845                    |
| SG-5          | 30.27          | 3.881 | 3.861 | 11.632 | 174.300    | 0.2583                    |
| SG-10         | 29.25          | 3.872 | 3.841 | 11.624 | 172.876    | 0.4019                    |
| SG-20         | 27.66          | 3.871 | 3.842 | 11.611 | 172.683    | 0.3760                    |



The surface morphology and particle distributions of the generated samples were investigated using SEM images (Figures 2 and 3). Both SSR and SG samples had a porous structure and surface alterations brought on by the doping procedure, whereas SSR samples' surfaces were more porous. The samples have granular features and are orientated

randomly. Cobalt and iron impurities resulted in a reduction in porosity and modifications to particle boundaries. Nevertheless, there is an ideal doping level (0.05%) over which the grain boundaries erode and the surface morphology is negatively impacted.

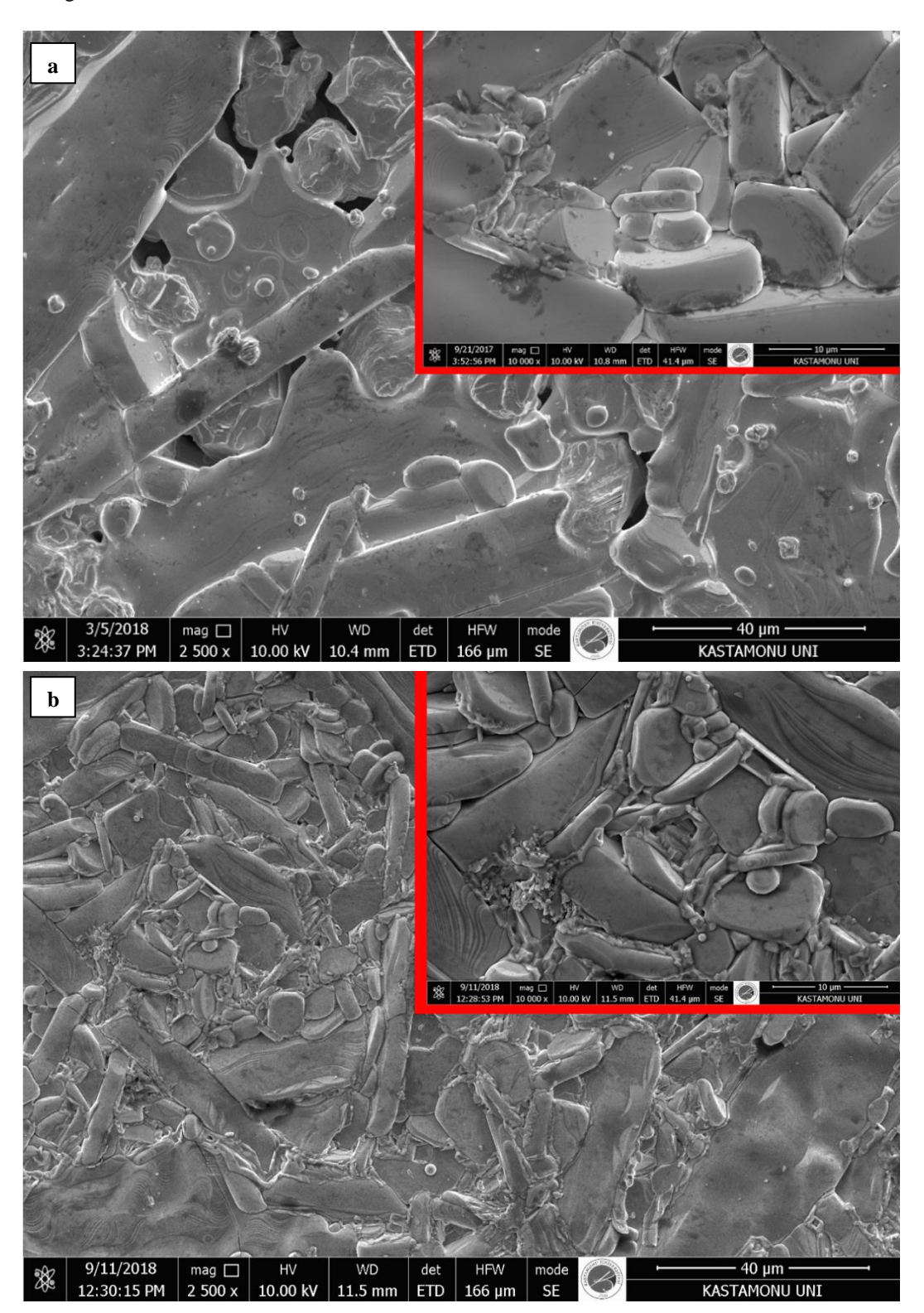


Figure 2. SEM images for a) SSR-0, b) SSR-5, c) SSR-10, d) SSR-20 samples produced by solid SSR.



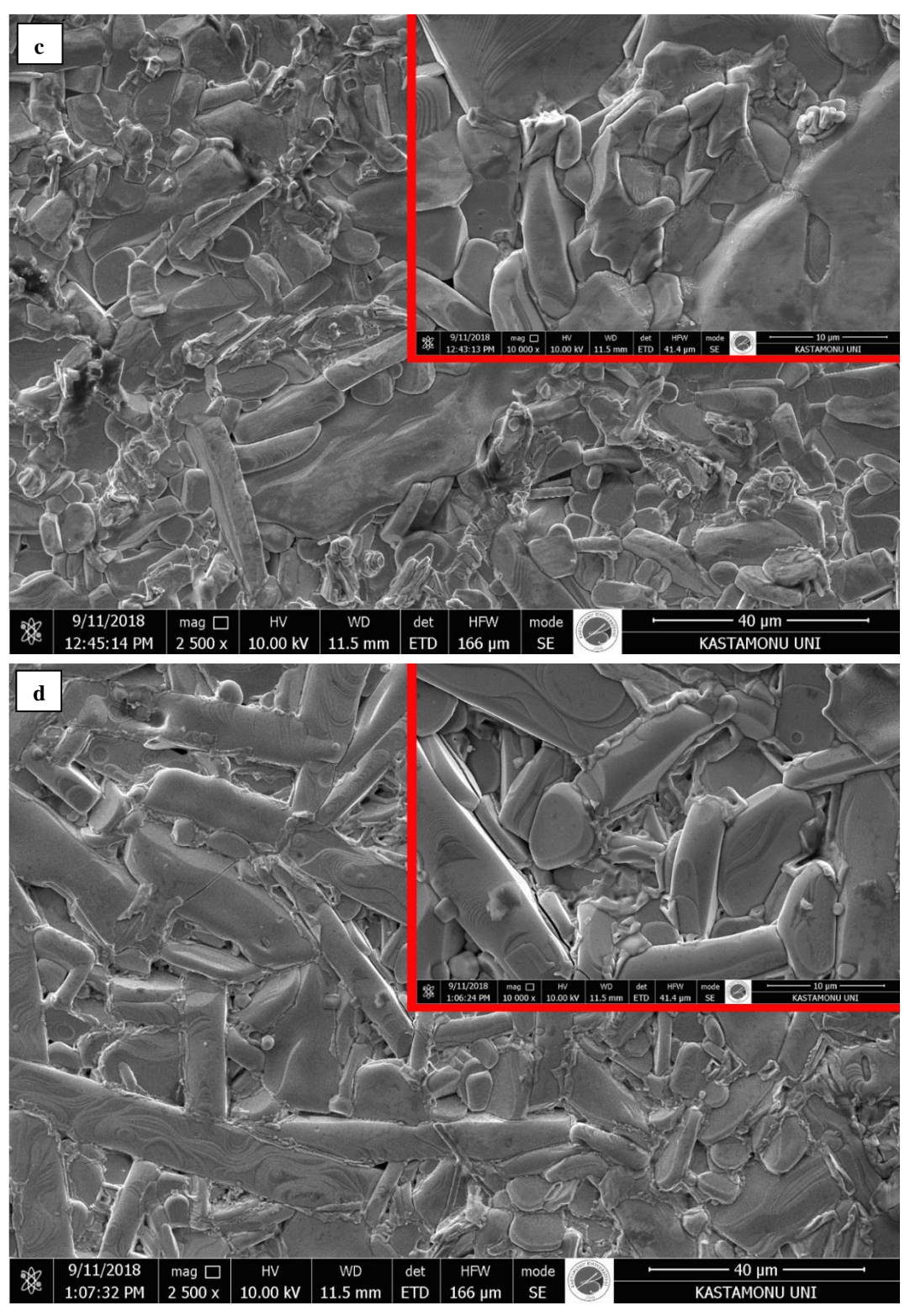


Figure 2. (continued).



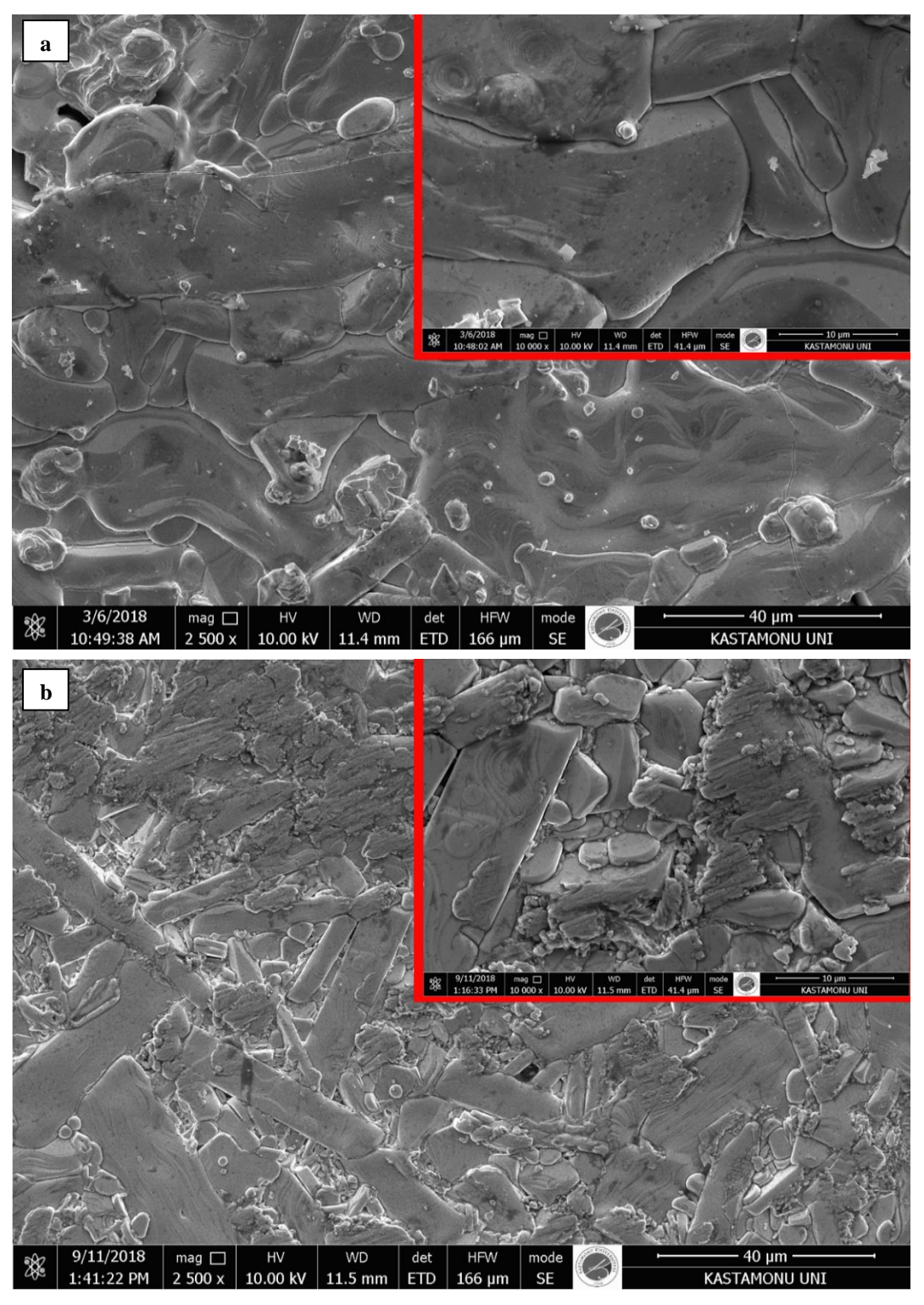


Figure 3. SEM images for a) SG-0, b) SG-5, c) SG-10, d) SG-20 samples produced by solid SG.

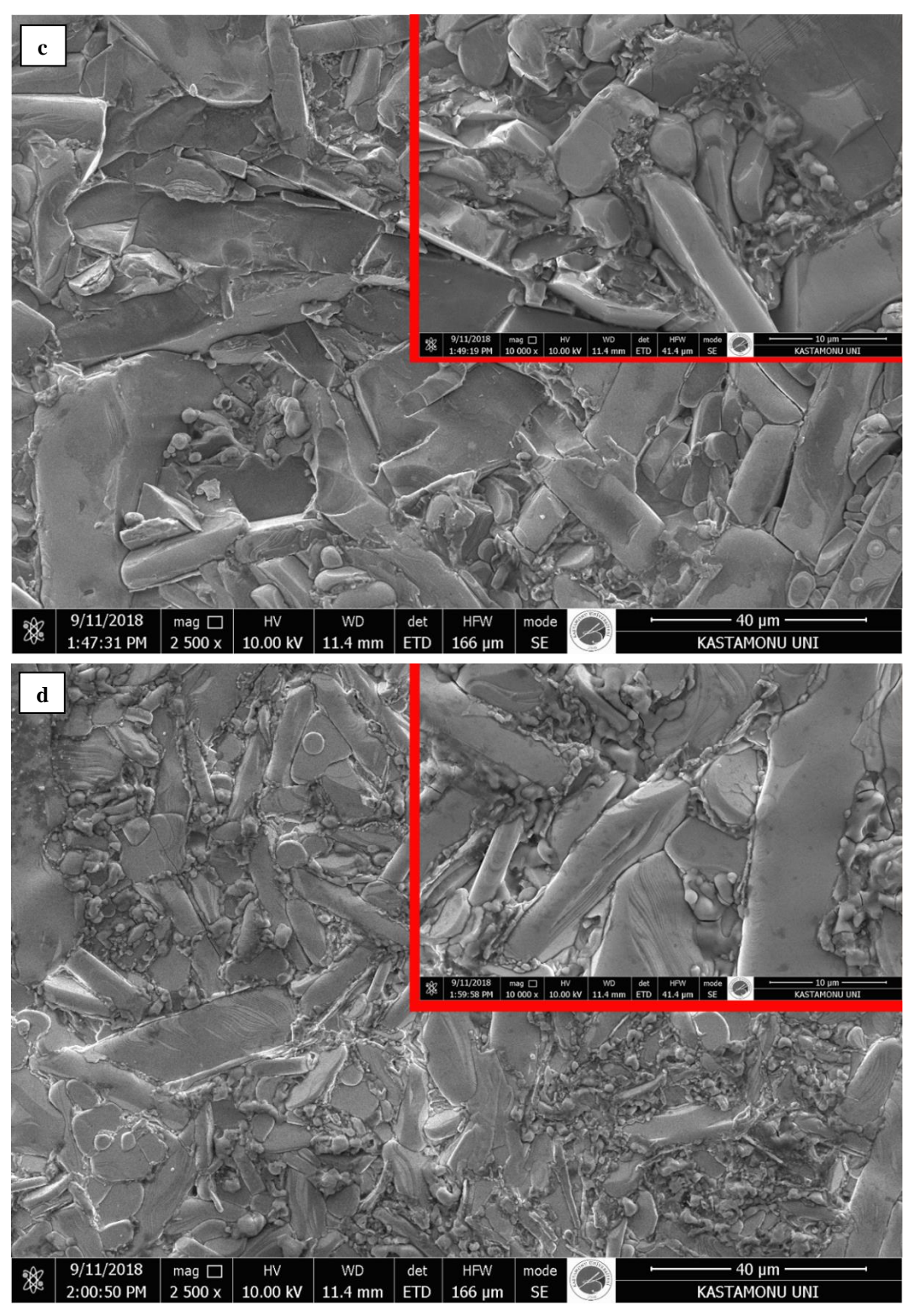


Figure 3. (continued).

## 3.2. Electrical Resistance Analysis

The samples were manufactured, and the electrical resistance measurements were done. Figure 4 shows the temperature dependency of the resistance graphs. The critical temperature values of the samples generated by solid state reaction technique are greater than those produced by sol-gel method, and SG-0 sample has shown lower critical temperature

value than the SSR-0 sample. The samples with the doping ratio have lower critical temperature values, and this is followed by a rise in the superconducting transition interval. This shows that the entry of cobalt and iron ions influences electron-phonon production, which, in turn, influences the concentration of holes in the CuO2 layer and results in a drop in the critical transition temperature with CoFe2O4 doping (Kuderowicz &



Wiendlocha, 2022). Moreover, the SG technique's  $T_C$  values are higher than those of the SSR method, showing that the SG method is more affected by the doping process (Table 2).

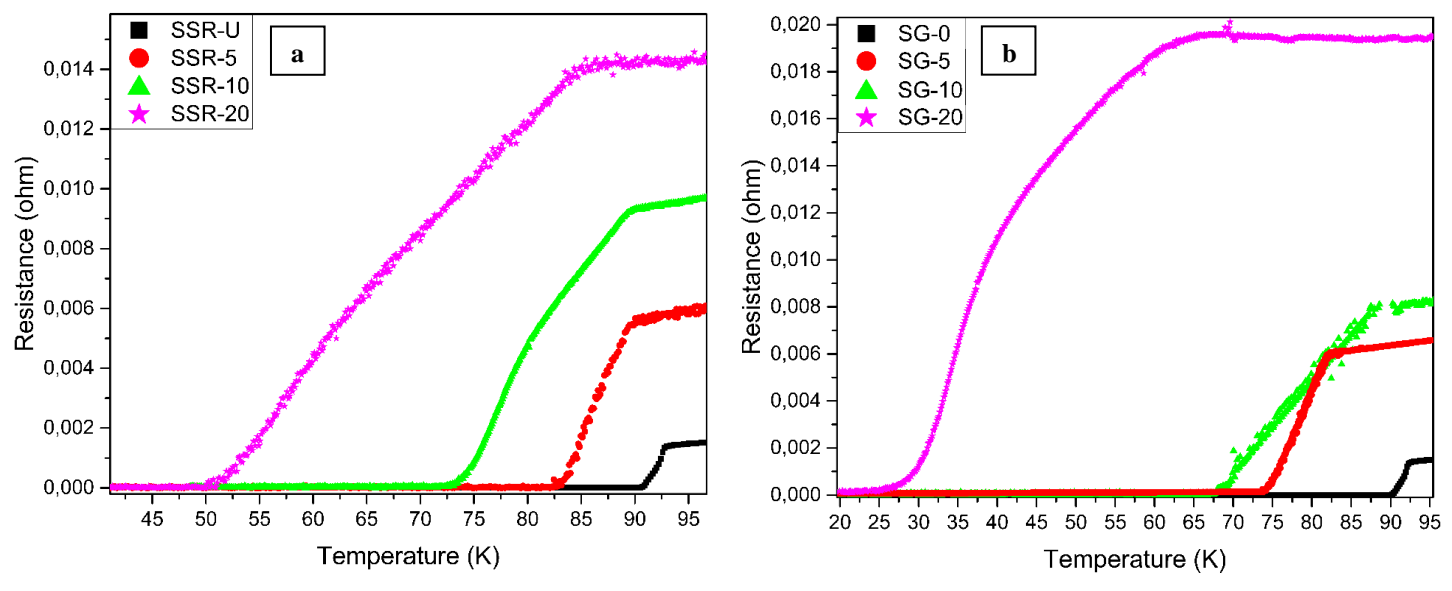


Figure 4. Temperature-dependent electrical resistance graph a) SSR, b) SG.

**Table 2.** Electrical resistance measurements of the produced samples.

| G 1           |                           | emperature (K)             | $\Delta T_{C}(\mathbf{K})$     |  |  |
|---------------|---------------------------|----------------------------|--------------------------------|--|--|
| Sample        | $T_{\mathcal{C}}^{onset}$ | $T_{\mathcal{C}}^{offset}$ | $(T_C^{onset} - T_C^{offset})$ |  |  |
| SSR-0         | 92.96                     | 90.29                      | 2.67                           |  |  |
| SSR-5         | 89.54                     | 83.15                      | 6.39                           |  |  |
| <b>SSR-10</b> | 89.26                     | 72.61                      | 16.65                          |  |  |
| SSR-20        | 83.97                     | 50.94                      | 33.03                          |  |  |
|               |                           |                            |                                |  |  |
| SG-0          | 92.46                     | 90.00                      | 2.46                           |  |  |
| SG-5          | 81.89                     | 73.93                      | 7.96                           |  |  |
| SG-10         | 89.08                     | 67.63                      | 21.45                          |  |  |
| SG-20         | 65.14                     | 25.31                      | 39.83                          |  |  |

# 3.3. Microhardness Analysis

Superconducting sample microhardness characteristics are crucial for assessing how well they may be used in industrial materials science and other technical domains. The Vicker's microhardness test is frequently used to evaluate these features, and key elements influencing the micro hardness properties include the sample fabrication process and the sample surface's reaction to the force that applied. The diagonal lengths obtained after applying five different loads to the sample surface for 10 seconds were used to calculate the hardness values of the samples created for this investigation. Calculations of Microhardness ( $H_V$ ), Elastic Modulus (E), and Yield Strength were used to assess mechanical characteristics (Y). Using Eqs. 5, 6, and 7, the  $H_V$  values were determined, correspondingly.

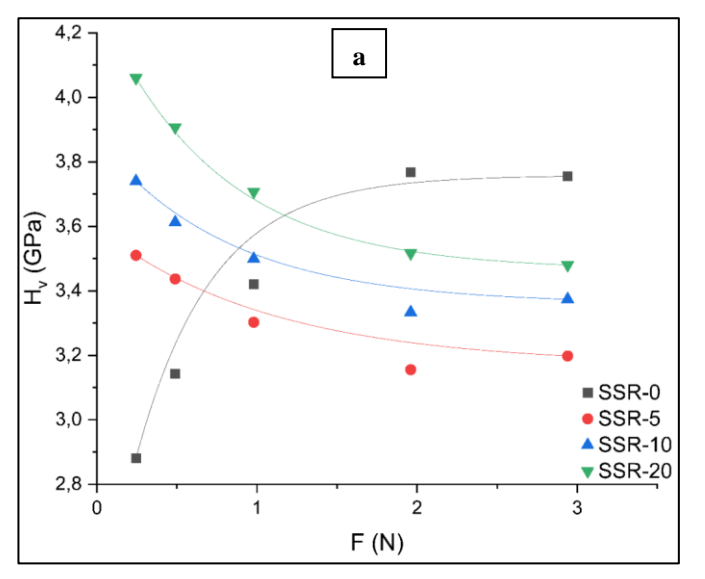
$$H_V = 1854.4 \left(\frac{F}{d^2}\right) \tag{5}$$

$$E = 81.9635 H_V \tag{6}$$

$$Y \approx H_V/3 \tag{7}$$

Vickers microhardness tests were performed on each sample, and estimated H<sub>V</sub>, E, and Y values for each sample under various test loads were obtained. When the load applied to the surface of the doped samples grows, the hardness values drop and the behavior of the ISE (Indentation Size Effect), which increases with increasing applied stress, is interpreted as the samples having attained saturation. The SG-20 sample with the greatest doping ratio was somewhat higher, while the SSR technique with the lowest doping rate revealed a little greater hardness rating than the undoped sample. The graphs from the experiments that are shown in Figure 5 and Table 3, respectively, as well as the variations between the two approaches, are the most crucial information. The undoped samples for both method present the RISE (Reverse Indentation Size Effect) feature, in which the microhardness values enlarged with enhancing applied stress (Yoshino et al., 2001; Awad et al., 2011). The creation of impurity, porosity, and weak bonding phases at the particle boundaries is thought to be the root cause of the change in microhardness behavior of samples as a result of the doping process (Dogruer et al., 2013; Zalaoglu et al., 2017).





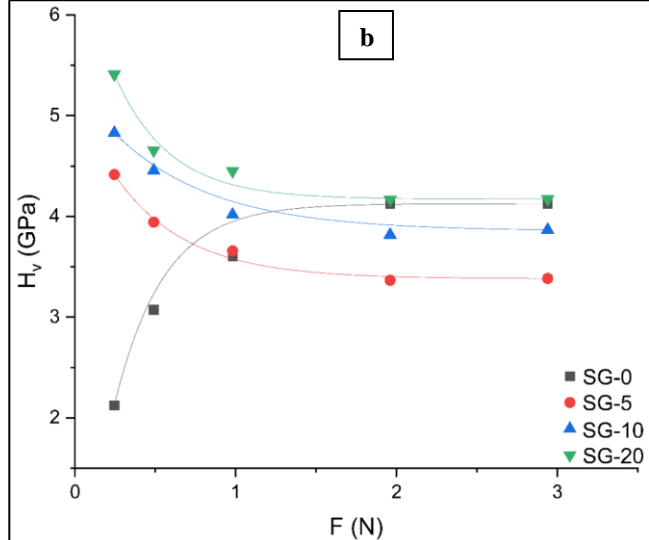


Figure 5. Vickers microhardness graph a) SSR, b) SG.

Table 3. Hardness parameters of samples such as; H<sub>V</sub>, E an Y.

| Sample        | F (N) | Hy (GPa) | E (GPa) | Y (GPa) | Sample | <b>F</b> ( <b>N</b> ) | Hv (GPa) | E (GPa) | Y (GPa) |
|---------------|-------|----------|---------|---------|--------|-----------------------|----------|---------|---------|
|               | 0.245 | 2.881    | 236.15  | 0.960   |        | 0.245                 | 2.126    | 174.254 | 0.709   |
|               | 0.490 | 3.143    | 257.63  | 1.048   |        | 0.490                 | 3.073    | 251.874 | 1.024   |
| SSR-0         | 0.980 | 3.420    | 280.28  | 1.140   | SG-0   | 0.980                 | 3.601    | 295.151 | 1.200   |
|               | 1.960 | 3.768    | 308.80  | 1.256   |        | 1.960                 | 4.122    | 337.854 | 1.374   |
|               | 2.940 | 3.755    | 307.80  | 1.252   |        | 2.940                 | 4.126    | 338.181 | 1.375   |
|               |       |          |         |         |        |                       |          |         |         |
|               | 0.245 | 3.510    | 287.712 | 1.170   |        | 0.245                 | 4.415    | 361.883 | 1.472   |
|               | 0.490 | 3.437    | 281.695 | 1.146   |        | 0.490                 | 3.943    | 323.204 | 1.314   |
| SSR-5         | 0.980 | 3.302    | 270.670 | 1.101   | SG-5   | 0.980                 | 3.658    | 299.799 | 1.219   |
|               | 1.960 | 3.155    | 258.617 | 1.052   |        | 1.960                 | 3.366    | 275.896 | 1.122   |
|               | 2.940 | 3.198    | 262.109 | 1.066   |        | 2.940                 | 3.384    | 277.343 | 1.128   |
|               |       |          |         |         |        |                       |          |         |         |
|               | 0.245 | 3.740    | 306.553 | 1.247   |        | 0.245                 | 4.829    | 395.815 | 1.610   |
|               | 0.490 | 3.612    | 296.083 | 1.204   | SG-10  | 0.490                 | 4.456    | 365.228 | 1.485   |
| <b>SSR-10</b> | 0.980 | 3.499    | 286.788 | 1.166   |        | 0.980                 | 4.017    | 329.242 | 1.339   |
|               | 1.960 | 3.334    | 273.228 | 1.111   |        | 1.960                 | 3.817    | 312.815 | 1.272   |
|               | 2.940 | 3.374    | 276.515 | 1.125   |        | 2.940                 | 3.867    | 316.921 | 1.289   |
|               |       |          |         |         |        |                       |          |         |         |
|               | 0.245 | 4.060    | 332.768 | 1.353   |        | 0.245                 | 5.410    | 443.425 | 1.803   |
|               | 0.490 | 3.907    | 320.243 | 1.302   | SG-20  | 0.490                 | 4.656    | 381.617 | 1.552   |
| <b>SSR-20</b> | 0.980 | 3.707    | 303.875 | 1.236   |        | 0.980                 | 4.449    | 364.685 | 1.483   |
|               | 1.960 | 3.516    | 288.216 | 1.172   |        | 1.960                 | 4.165    | 341.396 | 1.388   |
|               | 2.940 | 3.480    | 285.246 | 1.160   |        | 2.940                 | 4.172    | 341.944 | 1.391   |

# 3.4. Meyer's Law

The mechanical characteristic of ISE behavior that Meyber's mechanical modeling proposes is based on an empirical formula to explain: regular reduction of Vickers hardness parameters with applied external forces, or RISE, unusual enhancement of hardness values over the applied test loads for micro-indentation. Whereas the deformation in the material showing the RISE nature is only permanent, irreversible, and non-recoverable, the recoverable deformation

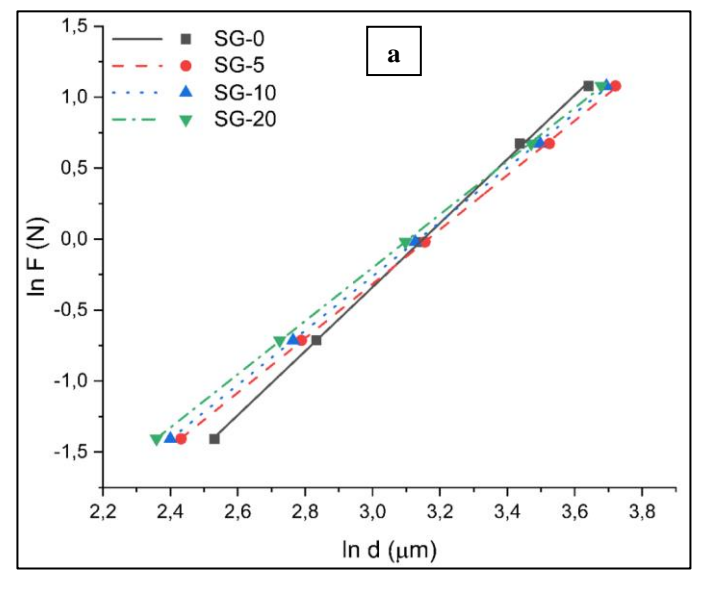
is temporary through the crystal system. The quantitative components of Meyer's law are the Meyer constant ( $A_{ML}$ ) and associated Meyer number (n), which has an exponential power for the indentation depth dependent on the stress applied to the surface. To describe the ISE or Rise behavior of material, N is found in three primary scales (n2, n=2, or n>2), with n2 being the first scale and 2 being the second scale. The Vickers microhardness results are unrelated to the indentation test load since n is equal to 8 (Toplu et al., 2015).



$$F = A_{ML}d^n (8)$$

Figure 6 shows the differentiation of LnF as a function of Lnd curves. Table 4 displays the numerical computations ( $A_{ML}$  relating to the y-axis crossing point and n derived from curve slope). Produced doped samples using either approach have n

values smaller than 2. Although the SG group offers the n values in the range of 1.814-2.668, the SSR group samples the n constant between 1.877 and 2.225. Doping the matrix with CoFe2O4 caused the mechanical behavior to shift from RISE to ISE.



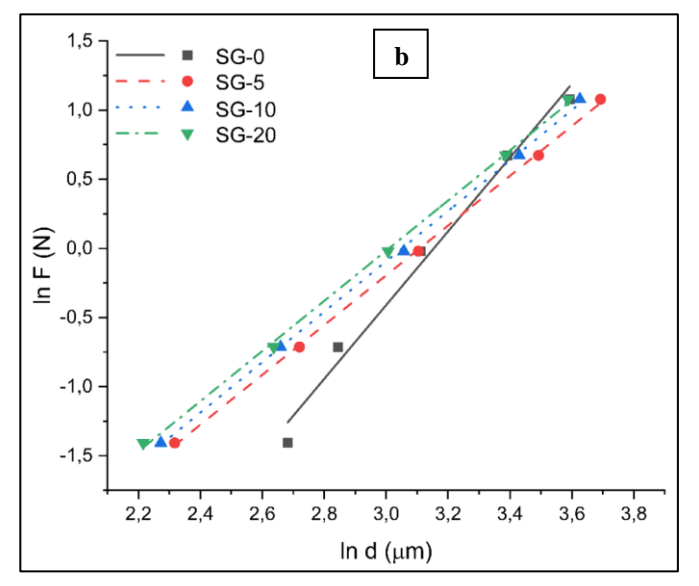


**Figure 6.** In F vs In d graphs of a) SSR, b) SG.

Table 4. Values that obtain from mechanical models.

|               | Meyer |        | HK     |         | EPD    |         | PSR       |           | IIC     |        |
|---------------|-------|--------|--------|---------|--------|---------|-----------|-----------|---------|--------|
|               | n     | A      | A*10^2 | W*10^2  | A*10^2 | d0*10^2 | alfa*10^2 | beta*10^2 | K       | m      |
| SSR-0         | 2.255 | -7.104 | 0.211  | -10.737 | 0.233  | -11.463 | -0.979    | 0.230     | 83.840  | 0.339  |
| SSR-5         | 1.916 | -6.064 | 0.170  | 3.292   | 0.164  | 3.754   | 0.318     | 0.163     | 0.074   | -0.400 |
| <b>SSR-10</b> | 1.912 | -5.997 | 0.179  | 3.451   | 0.173  | 3.900   | 0.339     | 0.172     | 0.056   | -0.440 |
| SSR-20        | 1.877 | -5.832 | 0.184  | 5.679   | 0.175  | 5.766   | 0.516     | 0.175     | 0.001   | -0.927 |
| SG-0          | 2.668 | -8.415 | 0.244  | -24.387 | 0.309  | -27.794 | -2.329    | 0.293     | 308.734 | 0.477  |
| <b>SG-5</b>   | 1.800 | -5.595 | 0.177  | 7.620   | 0.163  | 8.564   | 0.771     | 0.161     | 894.934 | 0.588  |
| SG-10         | 1.823 | -5.562 | 0.203  | 5.966   | 0.189  | 7.284   | 0.696     | 0.187     | 0.044   | -0.497 |
| SG-20         | 1.814 | -5.460 | 0.219  | 6.491   | 0.204  | 7.524   | 0.751     | 0.202     | 8.301   | 0.067  |

# 3.5. Hays-Kendall

The HK methodology is a popular technique for analyzing the fundamental mechanical properties and distinguishing characteristics of Y-123 ceramic compounds. The smallest critical load value that leads to form permanent deformation on the material is determined as W, and the mechanical characterization is determined with respect to the positive or negative value of W parameter. When the applied load is abbreviated as W, the  $A_{HK}$  parameter denotes the Vickers hardness value, and the  $A_{HK}$  and W constants are extrapolated from the curves. The pretreatment condition and partial Co/Cu substitution play crucial roles in delaying and preventing fracture propagation up to the terminal velocity at the applied test load.

$$F - W_{HK} = A_{HK}d^2 (9)$$

$$H_{HK} = (1854.4) A_{HK} \tag{10}$$

The HK methodology is a popular technique for analyzing the fundamental mechanical properties and distinguishing characteristics of Y-123 ceramic compounds. Equation 9's effective load is used to inspect the test load as a result of the variation in indentation depth size. The mechanical characterization is determined with respect to the positive or negative value of the W parameter, which is the minimum critical load value that causes the material to permanently deform. While W stands for the applied load, the  $A_{HK}$  parameter signifies the Vickers hardness value, and the  $A_{HK}$  and W constants are calculated from the curves using the data extrapolation method (Figure 7). Doped samples have positive W values, whereas undoped samples have negative W values.



The imposed test load precedes the negative W values that support permanent, irreversible, and non-recoverable deformation. The reported W values for doped materials were positive, showing that elastic and plastic deformation could be produced with a strong enough applied force (Rahal et al., 2017).

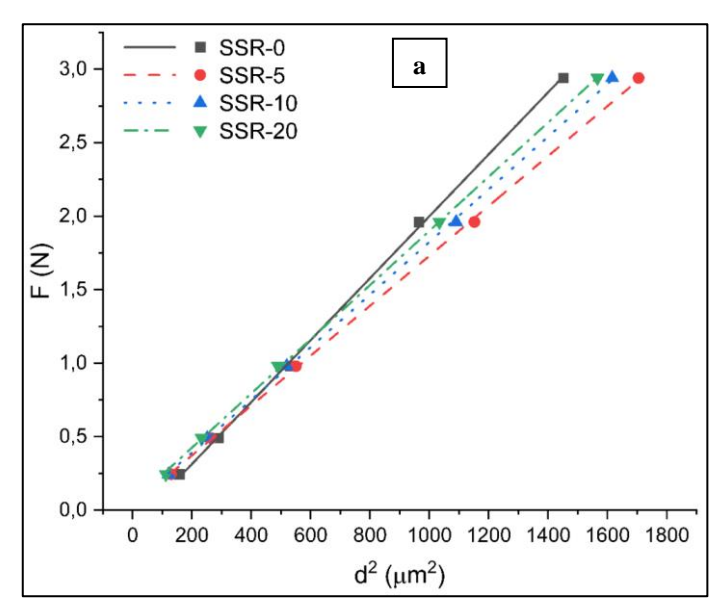


**Figure 7.** F vs  $d^2$  graphs of a) SSR, b) SG.

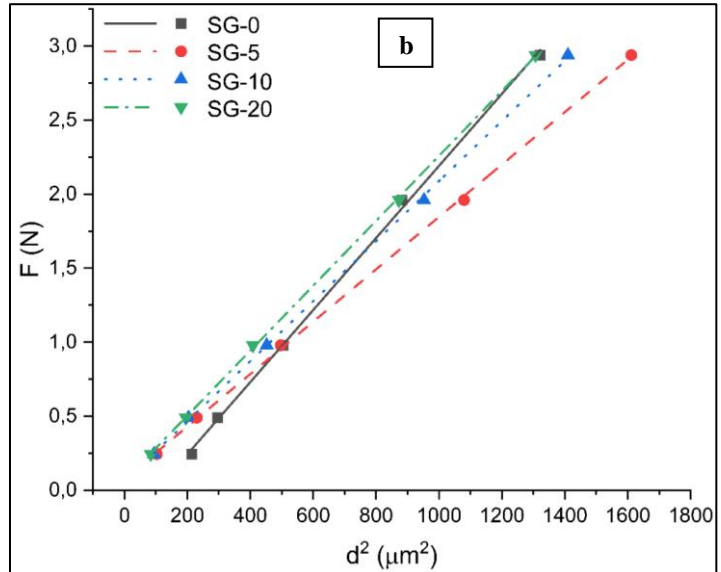
**Table 5.** Load dependent and independent microhardness values.

|               | Hv          | Ннк   | HEPD  | H <sub>PSR</sub> | Нпс   |
|---------------|-------------|-------|-------|------------------|-------|
| SSR-0         | 3,420-3,755 | 3.913 | 4.314 | 4.265            | 3.393 |
| SSR-5         | 3,198-3,302 | 3.152 | 3.037 | 3.023            | 3.320 |
| <b>SSR-10</b> | 3,374-3,499 | 3.319 | 3.200 | 3.190            | 3.511 |
| <b>SSR-20</b> | 3,480-3,707 | 3.412 | 3.251 | 3.245            | 3.734 |
| SG-0          | 3,601-4,126 | 4.525 | 5.731 | 5.433            | 3.410 |
| SG-5          | 3,384-3,658 | 3.282 | 3.025 | 2.986            | 3.734 |
| SG-10         | 3,867-4,017 | 3.764 | 3.496 | 3.468            | 4.181 |
| SG-20         | 4,172-4,499 | 4.061 | 3.780 | 3.746            | 4.549 |

#### 3.6. Elastic-plastic Deformation

A new word referring to the irreversible deformation comes in the formulation as a correlation factor. Because of this, it is proposed that when calculating microhardness using Equation 11, the plastic component of the  $d_E$  value be added to the deformation diagonal. As shown in Figure 8, the differentiation of  $F^{1/2}$  over d curves yields the constants of the  $A_{EPD}$  and  $d_E$  parameters. The computations that were done are shown in Table 4. In particular, it is shown that when the amount of  $CoFe_2O_4$  doping rises, the values of the  $d_E$  constants for the doped samples obtained by the SSR technique rise routinely. Moreover, equation 12 is used to get the load-independent hardness value for the elastic-plastic deformation model. The model is unable to check the general mechanical performance

Equation 10 in the HK model also examines the initial Vickers micro-indentation hardness values in the plateau limit area. The load-dependent Vickers micro-indentation hardness values are found to be lower than the  $H_V$  values, which are shown in Table 5, at the saturation limit areas. This implies that the HK method is insufficient for analyzing the initial microhardness values.



parameters in the plateau limit zone because the load-independent microhardness values estimated for the elastic deformation are found to be lower than those in the region (Table 5).

$$F = A_{EPD}(d + d_E)^2 \tag{11}$$

$$H_{EPD} = 1854.4 * A_{EPD} \tag{12}$$

## 3.7. Proportional Samples Resistance

Li and Bradt (1993) discovered the PSR theoretical approach as a further technique for investigating the initial microhardness values of a material displaying the ISE behavior, and in particular for demonstrating the difference in crystal structure quality based on the replacement process. Equation 13's parameters for surface energy and micro-indentation hardness are included in the PSR approach's relationship (Barakat et al., 2015). Equation 13's parameters for surface energy and micro-indentation hardness are included in the PSR approach's relationship (Barakat et al., 2015). Using the data extrapolation approach, the surface energy and microhardness constants of the materials are determined from the differentiation of F/d against d graphics in Figure 9; the resulting parameters, and are then numerically shown in Table 4. As can be observed from the picture, doped samples with positive values exhibit ISE behavior whereas SSR-0 and SG-0 samples with negative values exhibit atypical RISE behavior. For the SSR-5, SSR-10, and SSR-20 samples, respectively, it is

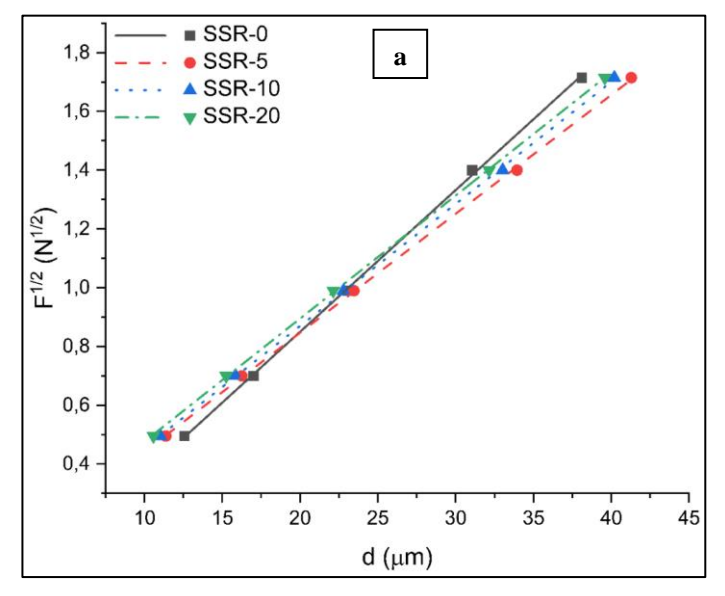


discovered that the value rises progressively. The theoretical PSR model, which uses equation 14, examines the load-independent microhardness characteristics in the plateau limits. For samples that were not doped, the results from the PSR model were found to be somewhat bigger than the actual

Vickers hardness parameters, but for samples that had been doped, they were found to be smaller.

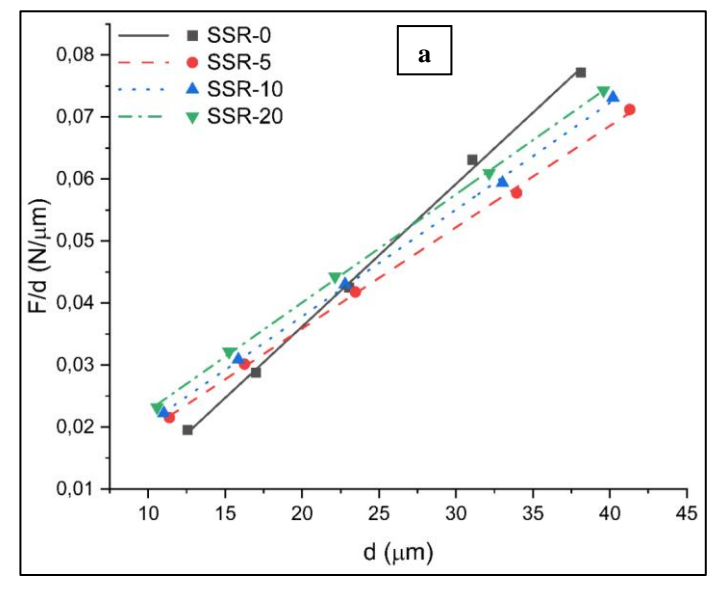
$$F = \gamma d + \beta d^2 \tag{13}$$

$$H_{PSR} = (1854.4)\beta \tag{14}$$



SG-0 1.8 b SG-5 SG-10 1,6 SG-20 1.4 F<sup>1/2</sup> (N<sub>1/2</sub>) 0,1 c,1 0,8 0,6 0.4 25 20 5 15 30 35 10 40 45 d (µm)

**Figure 8.**  $F^{1/2}$  vs d graphs of a) SSR, b) SG.



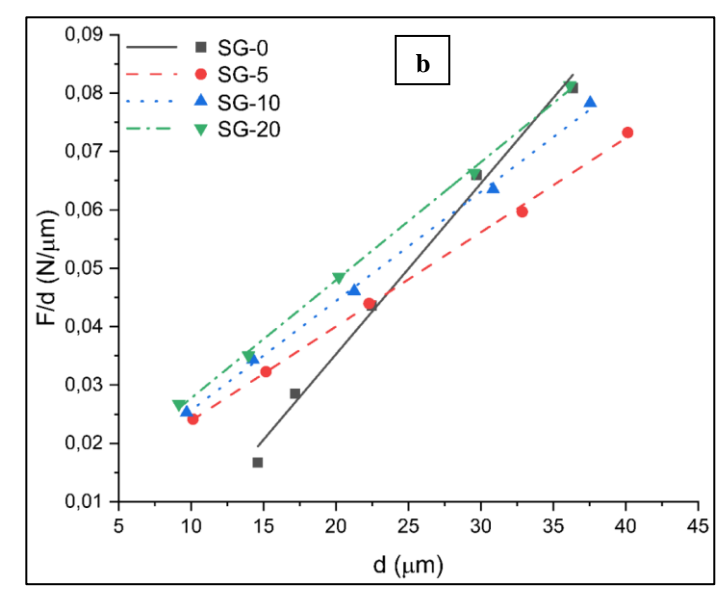


**Figure 9.** F/d vs d graphs of a) SSR, b) SG.

# 3.8. Indentation-induced Cracking

In order to investigate whether a material exhibits ISE or RISE behavior, the model is utilized to examine broad mechanical characteristic features. In this mechanical modeling calculation, the formation of indentation diagonal lengths is primarily based on four factors: (I) indenter friction; (II) and (III) elastic and plastic deformation; and (IV) crack mechanism. The relationship is represented by equation 15 and the relation is shown in the figure. The original Vickers microhardness constant, deduced from the curves shown in Figure 10's ln(Hv)

over ln(F5/3/d3), is represented by the abbreviations of the m and K constants in equation 15. For the CoFe2O4 doped samples produced by the SSR model, it has been shown that the values of K constants typically are noticed to drop systematically, improving the crystallinity of the materials. Another likely conclusion drawn from this most recent research is that the samples obtained had m constants that are less than 0.6, indicating that the ceramic compounds exhibit ISE behavior (Barakat et al., 2015). To examine the mechanical properties and features of CoFe2O4 doped polycrystalline Y-



123 ceramic materials, the IIC technique is clearly a key contender in this respect.

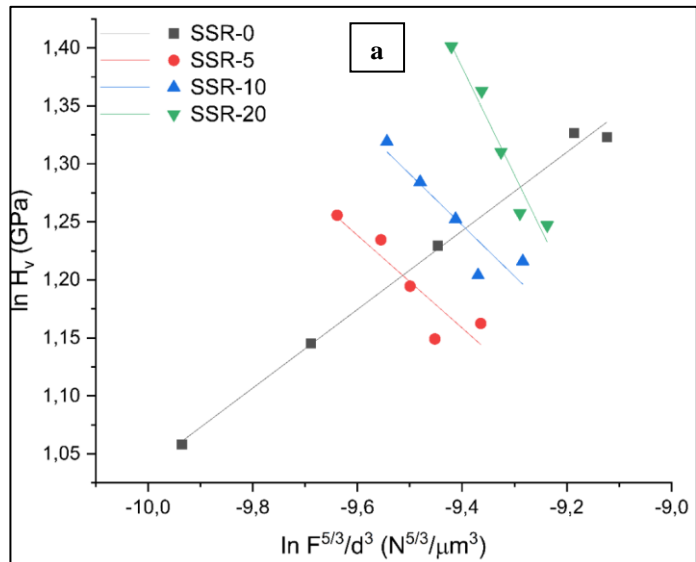
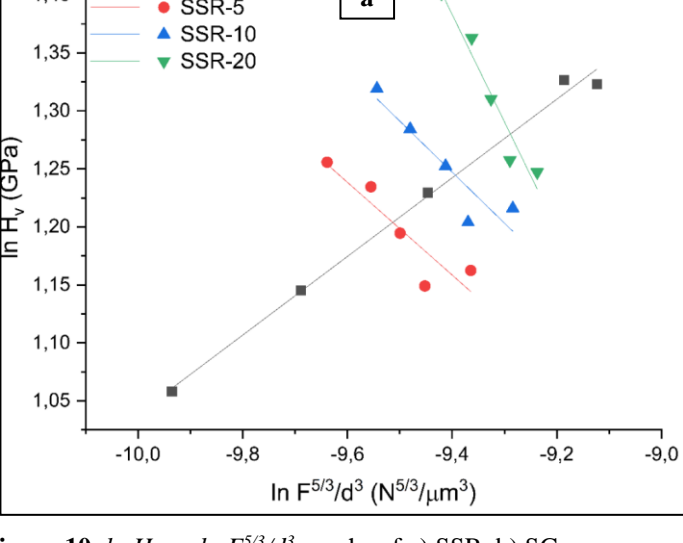


**Figure 10.**  $ln H_V$  vs  $ln F^{5/3}/d^3$  graphs of a) SSR, b) SG.



# 4. Conclusion

The SSR method was the most successful in preserving the orthorhombic structure of YBa<sub>2</sub>Cu<sub>3-x</sub>(CoFe<sub>2</sub>O<sub>4</sub>)<sub>x</sub>O<sub>7-δ</sub> copper based superconducting samples produced by solid state reaction and sol-gel methods. The samples showed higher T<sub>C</sub> values for the identical doping levels, according to an X-ray examination. Analyzing the impact of the manufacturing process and addition on the structure was also done. Both undoped samples showed RISE behavior, however due to variables such altered particle boundaries and porosity, ISE behavior was seen in doped samples. SSR was discovered to be more effective with softer materials.

## **Conflict of Interest**

The authors declare that they have no conflict of interest.

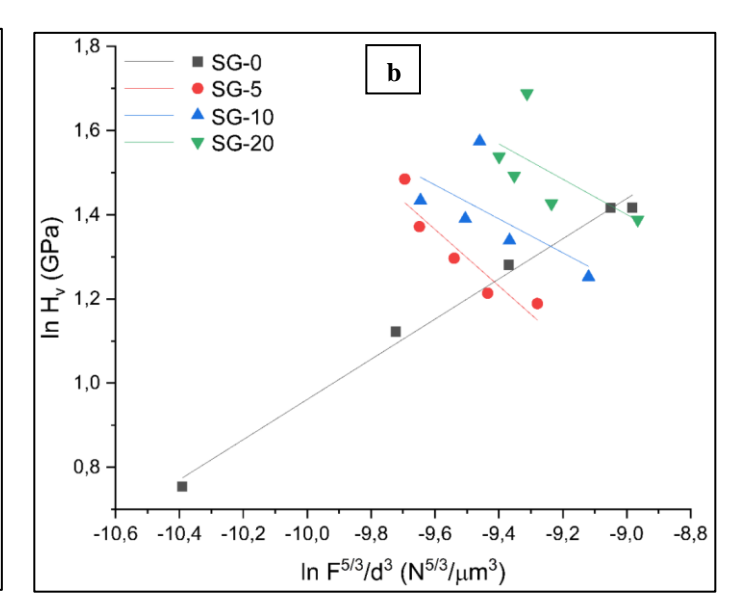
#### References

Awad, R., Abou Aly, A. I., Kamal, M., & Anas, M. (2011). Mechanical properties of (Cu0.5Tl0.5)-1223 substituted by Pr. Journal of Superconductivity and Novel Magnetism, 24, 1947-1956. https://doi.org/10.1007/s10948-011-1150-4

Aydıner, A., Çakır, B., Başoğlu, M., & Yanmaz, E. (2010). The effect of excess Y 2 O 3 addition on the mechanical properties of melt-processed YBCO superconductor. Journal of Superconductivity and Novel Magnetism, 23, 1493-1497. https://doi.org/10.1007/s10948-010-0801-1

Barakat, M. M. E., Abou-Aly, A. I., Awad, R., Aly, N. S., & Ibrahim, S. (2015). Mechanical properties of Y3-xNdxBa5-xCaxCu8O18-δ samples. Journal of





Alloys and Compounds, 652, 158-166. https://doi.org/10.1016/j.jallcom.2015.08.192

Dogruer, M., Gorur, O., Karaboga, F., Yildirim, G., & Terzioglu, C. (2013). Zr diffusion coefficient and activation energy calculations based on EDXRF measurement and evaluation of mechanical characteristics of YBa2Cu3O7-x bulk superconducting ceramics diffused with Zr nanoparticles. Powder Technology, 246, 553-560. https://doi.org/10.1016/j.powtec.2013.06.018

Feng, Y., Zhou, L., Shi, L., Lu, Y., Jin, X., Zhang, Y., Jin, J., Yao, X., & Zhang, Y. (1994). Study on the properties of Sn-added YBCO prepared by the powder melting process. Journal of Applied Physics, 76, 2954-2959. https://doi.org/10.1063/1.357535

Khalil, S. M. (2001). Enhancement of superconducting and mechanical properties in BSCCO with Pb additions. Journal of Physics and Chemistry of Solids, 62(3), 457-466. https://doi.org/10.1016/S0022-3697(00)00088-3

Koralay, H., Hicyilmaz, O., Cavdar, S., Asikuzun, E., Tasci, A. T., & Ozturk, O. (2014). Effect of Zn content on microstructure and mechanical performance Bi1.8Sr2Ca2Cu3.2-xZn xO10+δ glass ceramic. Journal of Materials Science: Materials in Electronics, 25, 3116-3126. https://doi.org/10.1007/s10854-014-1992-1

Kuderowicz, G., & Wiendlocha, B. (2022). The effect of Ni doping on the electronic structure and superconductivity in the noncentrosymmetric ThCoC2. Journal of Magnetism and Magnetic Materials, 546, 168688. https://doi.org/10.1016/j.jmmm.2021.168688

Leblond-Harnois, C., Caillard, R., Monot-Laffez, I., Desgardin, G., & Raveau, B. (2000). Texturing process,



- superconducting and mechanical properties of Agdoped top-seeded melt-grown YBCO pellets. *Physica C: Superconductivity*, 341–348, 2439–2440. https://doi.org/10.1016/S0921-4534(00)01161-8
- Li, H., & Bradt, R. C. (1993). The microhardness indentation load/size effect in rutile and cassiterite single crystals. *Journal of Materials Science*, 28, 917–926. https://doi.org/10.1007/BF00400874
- Rahal, H. T., Awad, R., Gaber, A. M. A., & Roumie, M. (2017). Superconducting and mechanical properties of the bulk (SnO2)x(Bi1.6Pb0.4)Sr2Ca2Cu3O10-δ prepared at different sintering times. *Journal of Superconductivity and Novel* Magnetism, 30, 1971–1980. https://doi.org/10.1007/s10948-016-3654-4
- Toplu, A., Karaca, İ., & Kölemen, U. (2015). Calculation of true hardness value of Zn added (BiPb)SrCaCuO superconductor by different models. *Ceramics International*, 41(1), 953–960. https://doi.org/10.1016/j.ceramint.2014.09.014
- Turkoz, M. B., Nezir, S., Terzioglu, C., Varilci, A., & Yildirim, G. (2013). Investigation of Lu effect on YBa2Cu3O 7-δ superconducting compounds. *Journal of Materials*

- *Science: Materials in Electronics*, 24, 896–905. https://doi.org/10.1007/s10854-012-0846-y
- Yeoh, L. M., & Ahmad, M. (2008). Characterization and synthesis of Y0.9Ca0.1Ba1.8Sr0.2Cu3O7–δ via combining sol–gel and solid-state route. *Journal of Non-Crystalline Solids*, 354(33), 4012–4018. https://doi.org/10.1016/j.jnoncrysol.2008.04.008
- Yilmaz, M., & Dogan, O. (2012). Structural and superconducting properties in Y0.6Gd0.4Ba2(Nb)Cu3O7-y cuprates doped with niobium. *Journal of Rare Earths*, 30(3), 241–244. https://doi.org/10.1016/S1002-0721(12)60031-3
- Yoshino, Y., Iwabuchi, A., Noto, K., Sakai, N., & Murakami, M. (2001). Vickers hardness properties of YBCO bulk superconductor at cryogenic temperatures. *Physica C: Supercond*, 357–360, 796–798. https://doi.org/10.1016/S0921-4534(01)00367-7
- Zalaoglu, Y., Karaboga, F., Terzioglu, C., & Yildirim, G. (2017). Improvement of mechanical performances and characteristics of bulk Bi-2212 materials exposed to Au diffusion and stabilization of durable tetragonal phase by Au. *Ceramics* International, *43*(9), 6836–6844. https://doi.org/10.1016/j.ceramint.2017.02.104

